AGU PUBLICATIONS

Geochemistry, Geophysics, Geosystems

RESEARCH ARTICLE
10.1002/2016GC006459

# Exploring the potential of clumped isotope thermometry on coccolith-rich sediments as a sea surface temperature proxy

**Anna Joy Drury[1,2] and Cédric M. John[1]**

[1]Department of Earth Science and Engineering, Imperial College London, London, UK, [2]Now at: MARUM—Center for Marine Environmental Sciences, University of Bremen, Bremen, Germany

**Key Points:**
- Clumped isotope $\Delta_{47}$ temperatures from four size fractions of equatorial coccolith-rich sediments range from 18 to 29°C
- The $<63$ $\mu$m $\Delta_{47}$ temperatures are comparable to coeval alkenone SSTs
- Clumped isotopes on appropriate coccolith-rich size fractions have potential as an SST proxy

**Supporting Information:**
- Supporting Information S1
- Table S1

**Correspondence to:**
A. J. Drury,
ajdrury@marum.de

**Citation:**
Drury A. J., and C. M. John (2016), Exploring the potential of clumped isotope thermometry on coccolith-rich sediments as a sea surface temperature proxy, *Geochem. Geophys. Geosyst.*, *17*, doi:10.1002/2016GC006459.

Received 27 MAY 2016
Accepted 27 SEP 2016
Accepted article online 29 SEP 2016

© 2016. American Geophysical Union. All Rights Reserved.

**Abstract** Understanding past changes in sea surface temperatures (SSTs) is crucial; however, existing proxies for reconstructing past SSTs are hindered by unknown ancient seawater composition (foraminiferal Mg/Ca and $\delta^{18}O$) or reflect subsurface temperatures ($TEX_{86}$) or have a limited applicable temperature range ($U^{k'}_{37}$). We examine clumped isotope ($\Delta_{47}$) thermometry to fossil coccolith-rich material as an SST proxy, as clumped isotopes are independent of original seawater composition and applicable to a wide temperature range and coccolithophores are widespread and dissolution resistant. The $\Delta_{47}$-derived temperatures from $<63$, $<20$, $<10$, and 2–5 $\mu$m size fractions of two equatorial Pacific late Miocene-early Pliocene sediment samples (c1; c2) range between ~18 and 29°C, with c1 temperatures consistently above c2. Removing the $>63$ $\mu$m fraction removes most nonmixed layer components; however, the $\Delta_{47}$-derived temperatures display an unexpected slight decreasing trend with decreasing size fraction. This unexpected trend could partly arise because larger coccoliths (5–12 $\mu$m) are removed during the size fraction separation process. The c1 and $<63$ $\mu$m c2 $\Delta_{47}$-derived temperatures are comparable to concurrent $U^{k'}_{37}$ SSTs. The $<20$, $<10$, and 2–5 $\mu$m c2 $\Delta_{47}$-derived temperatures are consistently cooler than expected. The $\Delta_{47}$-$U^{k'}_{37}$ temperature offset is probably caused by abiotic/diagenetic calcite present in the c2 2–5 $\mu$m fraction (~53% by area), which potentially precipitated at bottom water temperatures of ~6°C. Our results indicate that clumped isotopes on coccolith-rich sediment fractions have potential as an SST proxy, particularly in tropical regions, providing that careful investigation of the appropriate size fraction for the region and time scale is undertaken.

## 1. Introduction

Understanding past changes in sea surface temperatures (SSTs), particularly in tropical regions, is crucial to successfully reconstruct past climates, as SST distributions greatly influence both regional and global climate systems [*Zhang et al*., 2014]. Clumped isotope geochemistry is a thermometry technique based on the abundance of bonds between rare, heavy isotopes within a molecule (clumping), which is thermodynamically more favorable and therefore more prevalent at lower temperatures [*Eiler and Schauble*, 2004; *Schauble et al*., 2006]. This clumped isotope principle has been applied as a thermometer in carbonates, where the abundance of bonds between two rare $^{13}C$, $^{17}O$, and $^{18}O$ isotopes within the crystal lattice ($\Delta_{47}$) shows an inverse relationship across a wide range of temperature [*Ghosh et al*., 2006; *Schauble et al*., 2006; *Eiler*, 2007; *Kluge et al*., 2015]. A crucial benefit of $\Delta_{47}$ clumped isotope thermometry is that $\Delta_{47}$ is independent of the parent oxygen and carbon isotopic ($\delta^{18}O$ and $\delta^{13}C$) composition of the fluid [*Schauble et al*., 2006; *Eiler*, 2007]. The independence of $\Delta_{47}$ from fluid composition circumvents major issues with conventional stable isotope thermometers, as foraminiferal calcite $\delta^{18}O$ is controlled by original seawater $\delta^{18}O$ composition and species-specific vital effects, as well as temperature [*Urey*, 1947; *Epstein et al*., 1953; *Emiliani*, 1954; *Duplessy et al*., 1970; *Spero and Lea*, 1993].

Clumped isotope calibration studies were successfully applied to popular palaeoceanographic archives, including foraminifera, cultured coccoliths, and bulk core top sediments [*Tripati et al*., 2010; *Grauel et al*., 2013]. *Tripati et al*. [2010] showed that bulk core top samples show a similar $\Delta_{47}$-temperature relationship as the cultured coccolithophore and inorganic calcite. This similarity suggests that $\Delta_{47}$ measurements on coccoliths or coccolith-rich materials have great potential as a sea surface temperature proxy. Coccolithophores are small mixed-layer/photic zone phytoplankton, which have calcitic exoskeletons made up of many small platelets (coccoliths; 1–15 $\mu$m) [*Young et al*., 2005; *Schmidt et al*., 2006; *James and Austin*, 2008]. An SST proxy

based on the $\Delta_{47}$ of coccolith calcite is attractive, as coccolithophores are geographically and chronologically widespread, and because coccolith calcite is less receptive to dissolution than planktic foraminiferal calcite [*Schmidt et al*., 2006]. In addition, a $\Delta_{47}$-derived SST proxy could circumvent limitations of existing proxies that require assumption of prior fluid composition (foraminiferal $\delta^{18}O$ and Mg/Ca) [*Zhang et al*., 2014], reflect subsurface, not photic-zone, temperatures ($TEX_{86}$) [*Rommerskirchen et al*., 2011], or have upper temperature limits (~28°C for alkenone $U^{k'}_{37}$) [*Herbert*, 2003]. As $\Delta_{47}$-derived temperatures have no upper limit with respect to Earth surface temperatures, a coccolith-based $\Delta_{47}$-derived SST proxy could prove highly valuable in tropical regions.

Here we apply clumped isotope ($\Delta_{47}$) thermometry to fossil coccolith-rich materials, to explore its potential as an SST proxy. To achieve this, we: (1) investigate the influence and importance of isolating a specific sediment size fraction for the $\Delta_{47}$-derived temperatures; (2) compare the generated $\Delta_{47}$-derived temperatures to alkenone $U^{k'}_{37}$-derived temperatures to assess the potential of a coccolith-based $\Delta_{47}$-derived SST proxy. We use late Miocene-early Pliocene samples from equatorial Pacific Integrated Ocean Drilling Program (IODP) Site U1338 (Expedition 321), which can be compared to published alkenone-derived SST records from the same location for validation. By utilizing samples from the equatorial Pacific, we particularly aim to test the robustness of a coccolith-based $\Delta_{47}$-derived SST proxy in warm regions.

## 2. Materials and Methods

### 2.1. Paleoceanographical Setting (IODP Site U1338)

IODP Site U1338 (2°30.469′N, 117°58.178′W; water depth 4200 m, paleodepth ~3850–4050 m) was selected because of its location in the equatorial Pacific productivity belt during the late Miocene to early Pliocene and because of the recovery of an expanded composite section of calcareous nannofossil ooze with siliceous microfossils-rich sediment intervals [*Expedition 320/321 Scientists*, 2010; *Pälike et al*., 2010; *Wilkens et al*., 2013] (Figure 1). The late Miocene to early Pliocene interval is well documented at this location by published alkenone-derived ($U^{k'}_{37}$) SST, benthic, bulk, and 2–5 $\mu$m fraction $\delta^{18}O$ records [*Rousselle et al*., 2013; *Drury et al*., 2016]. Furthermore, scanning electron microscopy (SEM) studies show that coccoliths dominate the <63 $\mu$m fine fraction, although some etching removed central heterococcolith features and small amounts of secondary overgrowth are reported [*Drury et al*., 2014].

### 2.2. Sample Selection and Fine Fraction Separation

For this study, we chose two samples (c1 = 321-U1338B-8H-4-W 50/52 and c2 = 321-U1338B-11H-2-W 60/62; supporting information Table S1) that were selected based on their depth proximity to two samples analyzed by *Rousselle et al*. [2013]. This enables direct comparison of published $U^{k'}_{37}$ SST, bulk, and 2–5 $\mu$m fraction $\delta^{18}O$ records with the clumped isotope $\Delta_{47}$ and $\delta^{18}O$ results from this study (see supporting information Table S2 for depth and age offsets). Samples c1 and c2 were, respectively, selected close to a warmer and a cooler end-member of the late Miocene-early Pliocene $U^{k'}_{37}$ SST records, whilst remaining below the known upper temperature limit of $U^{k'}_{37}$. Choosing samples in close proximity to measured $U^{k'}_{37}$ data provides a unique opportunity to compare proxies on near-contemporaneous samples and minimizes problems caused by environmental differences that can occur when comparing different locations.

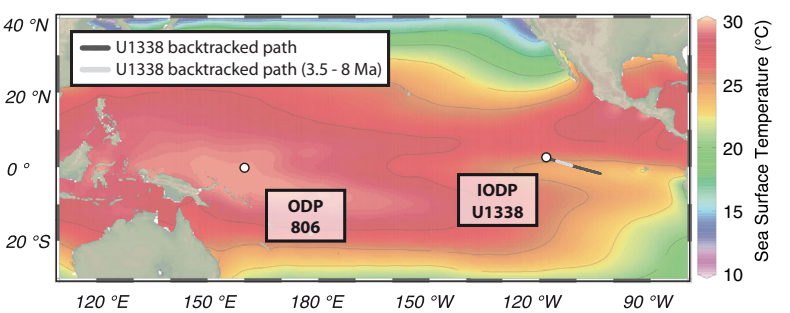



**Figure 1.** Locations of the sites discussed in this study, superimposed on modern sea surface temperatures [*Locarnini et al*., 2010]. New records were generated at IODP Site U1338, drilled during IODP PEAT Expedition 320/321 sites. The backtracked location of Site U1338 is shown as a dark grey line. The target interval between 8.0 and 3.5 Ma is shown in light grey (GeoMapApp [*Ryan et al*., 2009]).

Each sample (20 $cm^3$) was freeze dried, weighed, and 5 $cm^3$ archived. 15 $cm^3$ was wet sieved to separate the fine (<63 $\mu$m) and coarse (>63 $\mu$m) fractions and oven dried at 45°C. One gram of the <63 $\mu$m fractions were wet sieved through a 20 $\mu$m steel-mesh sieve with deionized (DI) water to isolate the <20 $\mu$m fraction. Half of the <20 $\mu$m fraction was washed through a 10 $\mu$m stainless steel-mesh sieve to isolate the <10 $\mu$m fraction. The 2–5 $\mu$m fraction was isolated by centrifugation-aided settling, which utilizes Stokes law:

$$V = \frac{g\ (\rho_p - \rho_l)\ D^2}{1.8\ \eta} \quad (1)$$

where V (m/s) is the terminal settling velocity of a particle, g is the gravitational constant (9.8 $m/s^2$), $\rho_p$ and $\rho_l$ are, respectively, the particle (2.70 $kg/m^3$ for calcite) and liquid (1.00 $kg/m^3$ for DI water) density, D is the spherical particle diameter in cm and $\eta$ (0.098 kg/(s m) at 21°C) is the liquid viscosity [*Moore and Reynolds*, 1997].

One gram of the <63 $\mu$m fraction was centrifuged in DI water to isolate the <5 $\mu$m fraction in the supernatant fluid and to remove the 5–63 $\mu$m fraction in the substrate: after 1 min at 500 RPM in 15 mL tubes, the supernatant fluid from 11.5 to 5 mL that contained the <5 $\mu$m particles was collected. This supernatant fluid was transferred and centrifuged again (2.5 min at 500 RPM in 15 mL tubes) to collect particles between 2 and 5 $\mu$m in the substrate (below 2 mL). Each centrifugation step was repeated eight times to collect sufficient material in the 2–5 $\mu$m fraction.

### 2.3. SEM and Area Analyses

SEM imaging was used to assess the success of the size fraction separation. The <20, <10, and 2–5 $\mu$m c1 and c2 size fractions samples were mounted with sticky carbon tape and imaged using a Leo 1455 VP (variable pressure) SEM at the Natural History Museum (London, UK) in back-scattered electron topography mode (BSE) (working distance = 15–16 mm; spot size setting = 500 (Leo 1455 VP-specific setting); acceleration voltage = 15 kV). To resolve the smallest components, the sample c2 2–5 $\mu$m fraction was platinum coated (coating thickness = 3 nm) and imaged using the JEOL JCM-6000 NeoScope Benchtop SEM at Utrecht University (the Netherlands) in high vacuum mode using secondary electron mode (SE) (working distance = 19 mm; filament and probe currents = high; acceleration voltage = 10 or 15 kV). In addition, energy dispersive X-ray spectroscopy (EDS) area maps were made of the 2–5 $\mu$m fraction of sample c2 (acceleration voltage = 15 kV; high filament and probe currents). Full-resolution versions of all SEM images are available in the online version.

To investigate the composition of the calcite in the 2–5 $\mu$m fraction of sample c2, four EDS maps were measured. The four calcium (Ca) EDS maps, taken as representative of calcite, were then further analyzed in Adobe Illustrator CS5 to provide a first-order estimate of the ratio of coccolith versus noncoccolith calcite. Each Ca-EDS map was traced using the live-trace function in Illustrator CS5, and the total trace area was calculated using the Telegraphics Patharea Filter plugin (http://telegraphics.com.au/sw/product/patharea; downloaded on 7 November 2013). Clearly identifiable coccoliths and coccolith fragments were traced by hand, and the total traced coccolith area estimated using the Patharea Filter. Per map, the ratio between the total calcite area and the traced coccolith area was used as the ratio of noncoccolith to coccolith calcite. The ratio of noncoccolith to coccolith calcite for the total sample is estimated using the average of the ratios from all four maps, with the standard deviation as a measure of uncertainty. This area analysis can help investigate the composition and source of the calcareous components of the 2–5 $\mu$m fraction of sample c2. This analysis was chosen as the best approach to deal with the c2 sample, as the samples from Site U1338 contain both siliceous and calcareous micro- and nannofossils that cannot be separated. By performing an area analysis of the Ca EDS maps alone, we exclude the siliceous components in later calculations. We do not account for superposition of particles and we assume that the particle's surface area is proportional to the particle's volume in this 2-D approach. This may underestimate the contribution of foraminiferal fragments, as these are generally thicker than coccoliths. The effects of these and other caveats are considered further in the discussion.

### 2.4. Clumped Isotope ($\Delta_{47}$) Analysis

The clumped isotope thermometer is defined by the $\Delta_{47}$ parameter, which quantifies the amount of multiply substituted mass 47 isotopologues of $CO_2$ compared to a stochastic distribution [*Eiler and Schauble*, 2004; *Huntington et al*., 2009]:

$$\Delta_{47}=\left[\frac{R^{47}}{2R^{13}\cdot R^{18}+2R^{17}\cdot R^{18}+R^{13}\cdot\left(R^{17}\right)^2}-\frac{R^{46}}{2R^{18}+2R^{13}\cdot R^{17}+\left(R^{17}\right)^2}-\frac{R^{45}}{R^{13}+2R^{17}}+1\right]\cdot 1000 \quad (2)$$

The $\Delta_{47}$ value is calculated using the measured ratios of masses 45, 46, and 47 to mass 44 ($R^{45}$, $R^{46}$, $R^{47}$), the $R^{13}$ ($^{13}C/^{12}C$) and $R^{18}$ ($^{18}O/^{16}O$) are calculated from $R^{45}$ and $R^{46}$ assuming a random distribution, and the $R^{17}$ is calculated from $R^{18}$ assuming a mass-dependent relationship between $^{18}O$ and $^{17}O$.

Three to four replicate measurements were run for each of the four size fractions (<63, <20, <10, and 2–5 $\mu$m) from samples c1 and c2. All measurements were done in the Qatar Stable Isotope laboratory at Imperial College London. Each replicate was reacted under vacuum with 105% orthophospohoric acid at 90°C and the captured $CO_2$ was cleaned using a manual vacuum line method similar to *Dennis and Schrag* [2010] and first described for the Imperial College laboratory in *Dale et al*. [2014]. The cleaned $CO_2$ was measured on a duel-inlet Thermo MAT 253 isotope ratio mass spectrometer using the method of *Huntington et al*. [2009].

The raw data were corrected using acid fractionation factors for calcite reactions at 90°C: 1.008128581 for $\delta^{18}O$ from *Kim et al*. [2007] and +0.069‰ for $\Delta_{47}$ from *Guo et al*. [2009] and *Wacker et al*. [2013]. Sample $\delta^{13}C$ and $\delta^{18}O$ values were corrected to Vienna Peedee Belemnite (VPDB) with a correction factor based on a 4 week average of the carbonate standards ETH3 and Carrara marble (Carrara marble [*Dennis et al*., 2011]; ISO C [*Meckler et al*., 2014]). The $\Delta_{47}$ measurements were corrected for nonlinearity using the heated gas method [*Huntington et al*., 2009]. All data were transferred into the Carbon Dioxide Equilibrated Scale (CDES) defined by *Dennis et al*. [2011] using the intercept of the heated gas line and the carbonate standards. The mass 48 and 49 parameters of each measurement were used to assess contamination [*Huntington et al*., 2009; *Dale et al*., 2014]: measurements with $\delta^{48}$ and $\Delta_{48}$ values plotting outside ±2‰ of the heated gas line were excluded, as well as samples with a 49-parameter greater than 0.2.

The final, corrected $\Delta_{47}$ replicates were averaged per sample size fraction, and reported with 1 standard error in ‰. $\Delta_{47}$ was converted to temperature using the calibration from *Kluge et al*. [2015], which reports values in the CDES and was developed in the same laboratory with the same methods and instruments as this study. The maximum calibration error for the [*Kluge et al*., 2015] is ~3°C, for the expected temperature range of this study (15–30°C). The *Kluge et al*. [2015] calibration was preferentially selected over calibrations from *Tripati et al*. [2010] and *Grauel et al*. [2013], because neither the Tripati or Grauel calibrations are reported in the CDES. Therefore, although the calibrations incorporate $\Delta_{47}$-temperature results from planktic foraminifera and coccolithophores, the results cannot directly be compared to the results from this study.

## 3. Results

### 3.1. BSE- and SE-SEM Imaging: Assessment of Separation Technique

SEM images of the different size fractions from both samples are shown in Figure 2. Whole foraminiferal tests were successfully removed by the sieving techniques, as these are no longer present in the <63 $\mu$m fraction (Figures 2a and 2e). The <20 $\mu$m fraction samples contain some large radiolarian fragments and diatoms (Figures 2b and 2f), however the amount is greatly reduced compared to the <63 $\mu$m fractions (Figures 2a and 2e), and almost no large fragments or diatoms remain in the <10 $\mu$m fractions (Figures 2c and 2g). The 2–5 $\mu$m fraction samples contain many heterococcoliths, as well as small foraminiferal and/or coccolith fragments; however, some larger diatom particles remained after centrifugation (Figures 2d, 2h, and 3). There are also large numbers of smaller particles (<2 $\mu$m) present in all size fractions (Figures 2 and 3).

### 3.2. EDS Maps and Area Analysis

Overlays of the calcium (Ca), silicon (Si) and barium (Ba) EDS maps on the topographic SEM images are shown in Figure 4. The $SiO_2$ present in the sample is predominantly within biogenic fragments of diatoms and radiolarians (green areas—Figures 4a and 4b). The remaining components of the sediment fraction are all calcitic, including the smaller (<2 $\mu$m) fragment (red area—Figures 4a and 4b).

Figure 5 shows the four Ca-EDS maps for the 2–5 $\mu$m fraction of sample c2. The red area shows the total calcite content, and components that are clearly identifiable as heterococcoliths are highlighted in yellow. In three of the four maps, more than 50% of the sample area is composed of coccolith calcite, whereas the last area only contains around 25% coccolith calcite (Figure 5). The average proportion of coccolith-calcite within the samples is ~47 ± 15%.

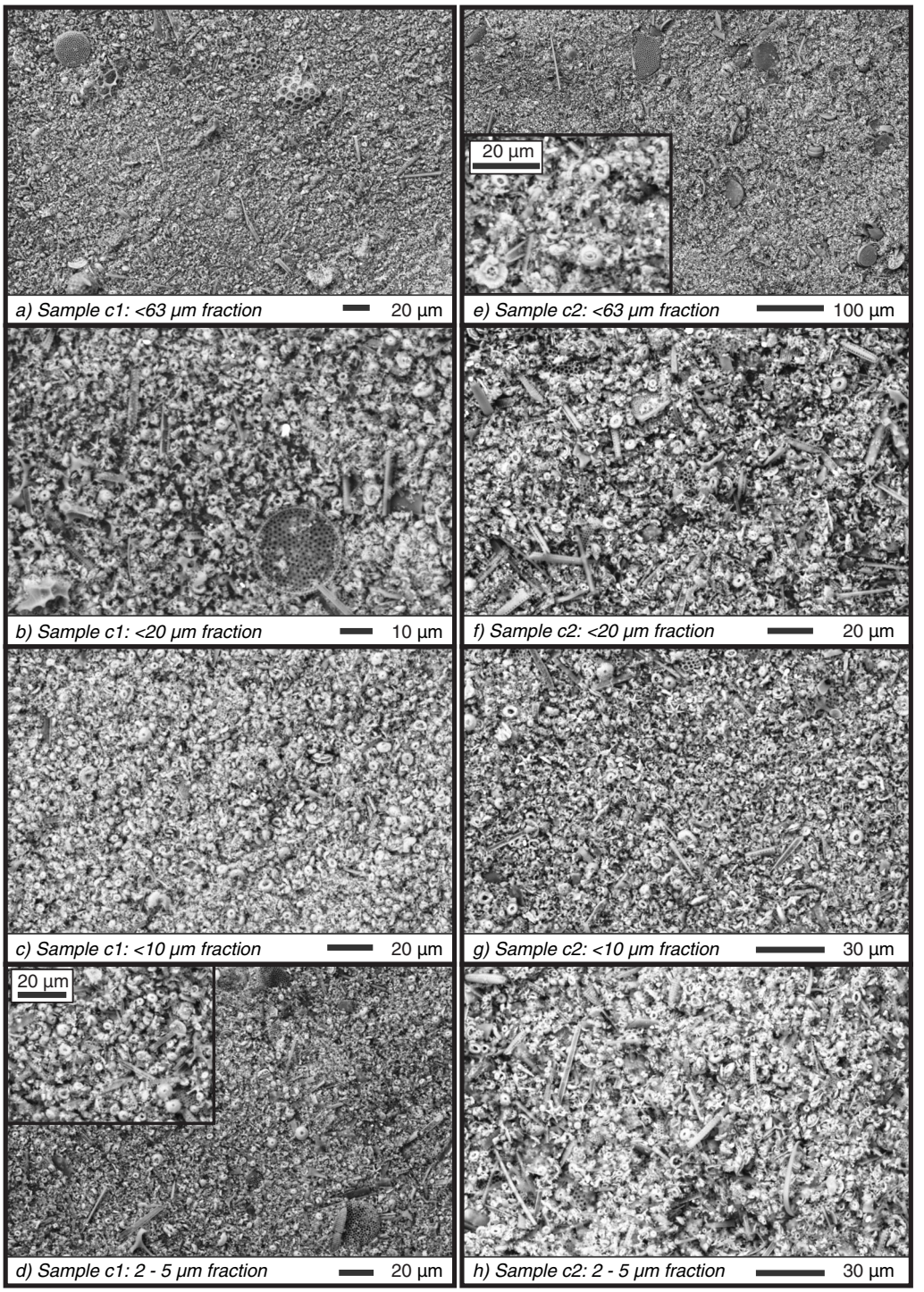



**Figure 2.** BSE-SEM images of the (a–d) c1 and (e–h) c2 samples. Inserts in Figures 2d and 2e show magnified sections of the same sample. Each size fraction was imaged separately. The images show that the size fraction separation was generally successful at removing most large fragments. Figures 2a and 2e come from *Drury et al.* [2014].

### 3.3. Conventional ($\delta^{18}O$, $\delta^{13}C$) and Clumped ($\Delta_{47}$) Isotopes and $\Delta_{47}$ Temperatures

All $\delta^{18}O$, $\delta^{13}C$, and $\Delta_{47}$ results are shown in supporting information Table S1. The $\delta^{18}O$ results for all size fractions of both samples c1 and c2 are within a single standard deviation (Figure 6a). The $\delta^{13}C$ results for each sample are not within a single standard deviation, although the difference between the size fractions

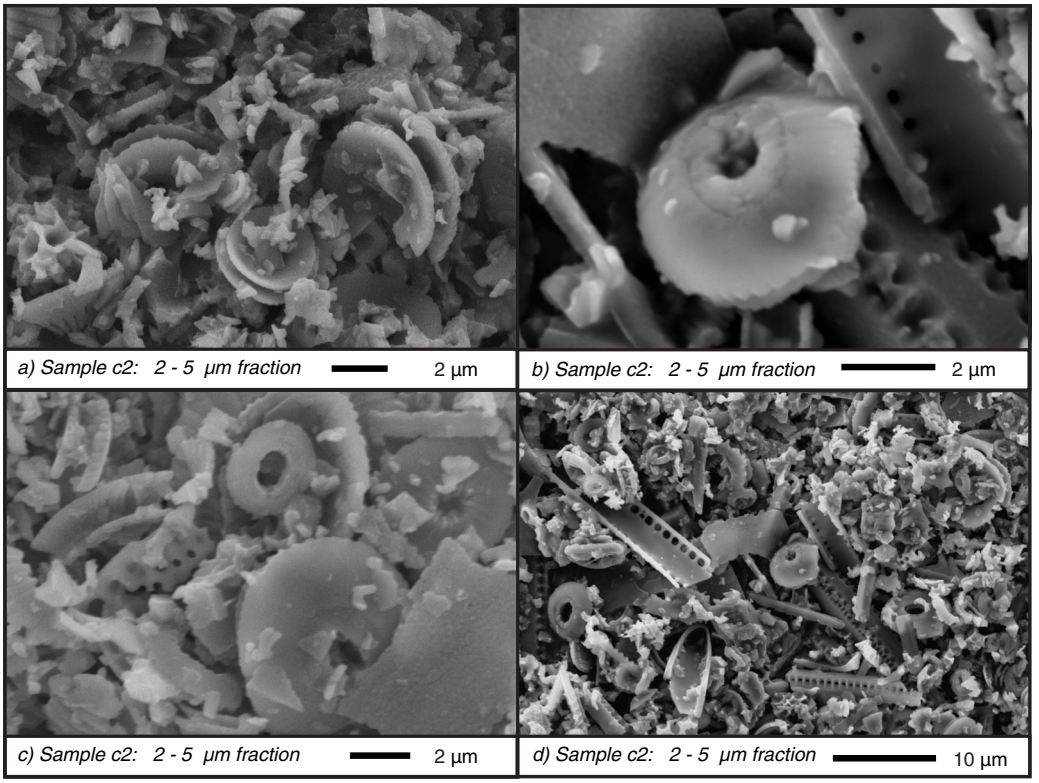



**Figure 3.** SE-SEM images of the c2 sample 2–5 $\mu$m size fraction, showing the presence of large numbers of coccoliths, as well as foraminiferal and/or coccolith fragments. The images also show small ($<2$ $\mu$m) fragments of unknown origin that could be fragments of holo- and/or heterococcoliths. Generally, there is slight to minor etching of the coccoliths. Original microstructures are retained, but there is some evidence of calcite overgrowths. Figure 3a is taken from *Drury et al.* [2014].

is very small ($\sim$0.1‰; Figure 6b). The average $\delta^{13}$C is offset by $\sim$0.8‰ between sample c1 and c2. Both samples show a slight increase in $\delta^{13}$C with decreasing size fraction between the $<$63 and 2–5 $\mu$m fractions (Figure 6).

The average $\Delta_{47}$ values for both samples c1 and c2 show a slight increasing trend, although the c1 values are all largely within standard error (Figure 6d and supporting information Table S2). For sample c2, the average $\Delta_{47}$ values of the two smallest size fractions ($<$10 and 2–5 $\mu$m) are slightly higher and not within error of the $<$63 and $<$20 $\mu$m fractions. The $\Delta_{47}$ values for c2 are consistently lower than the c1 $\Delta_{47}$ values for the $<$20 $\mu$m and smaller size fractions (Figures 6c and 6d). The $\Delta_{47}$-derived temperatures for sample c1 are consistently warmer than for sample c2 (supporting information Table S2 and Figures 6e and 6f).

## 4. Discussion

### 4.1. Effect of Size Fraction Separation on $\Delta_{47}$ Values

The sieve-based separation method successfully removed the larger fragments from the smaller fractions (Figures 2a–2c and 2e–2g). However, the centrifugation technique did not remove all larger diatom fragments (Figures 2d and 2h). Stokes' law assumes all particles are spherical with an identical density, whereas diatoms are hollow and nonspherical. Both these properties will increase the likelyhood that some diatoms remain behind after centrifugation. Furthermore, siliceous diatoms have a slightly lower density (2.65 kg/m$^3$) than calcite (2.70 kg/m$^3$) used to calculate the settling time. The centrifugation technique also did not remove all of the very small $<$2 $\mu$m particles from the 2–5 $\mu$m fraction (Figure 3).

Approximately 47% of the 2–5 $\mu$m fraction of sample c2 consists of clearly identifiable coccolith calcite (Figure 5), which is $\sim$25% lower than the average 75% *Neolaerhabdaceae* species found in the 2–5 $\mu$m fraction by *Rousselle et al.* [2013]. This $\sim$25% difference probably arises because the centrifugation technique used in this study did not remove all the calcareous $<$2 $\mu$m particles. This suggests that a different separation

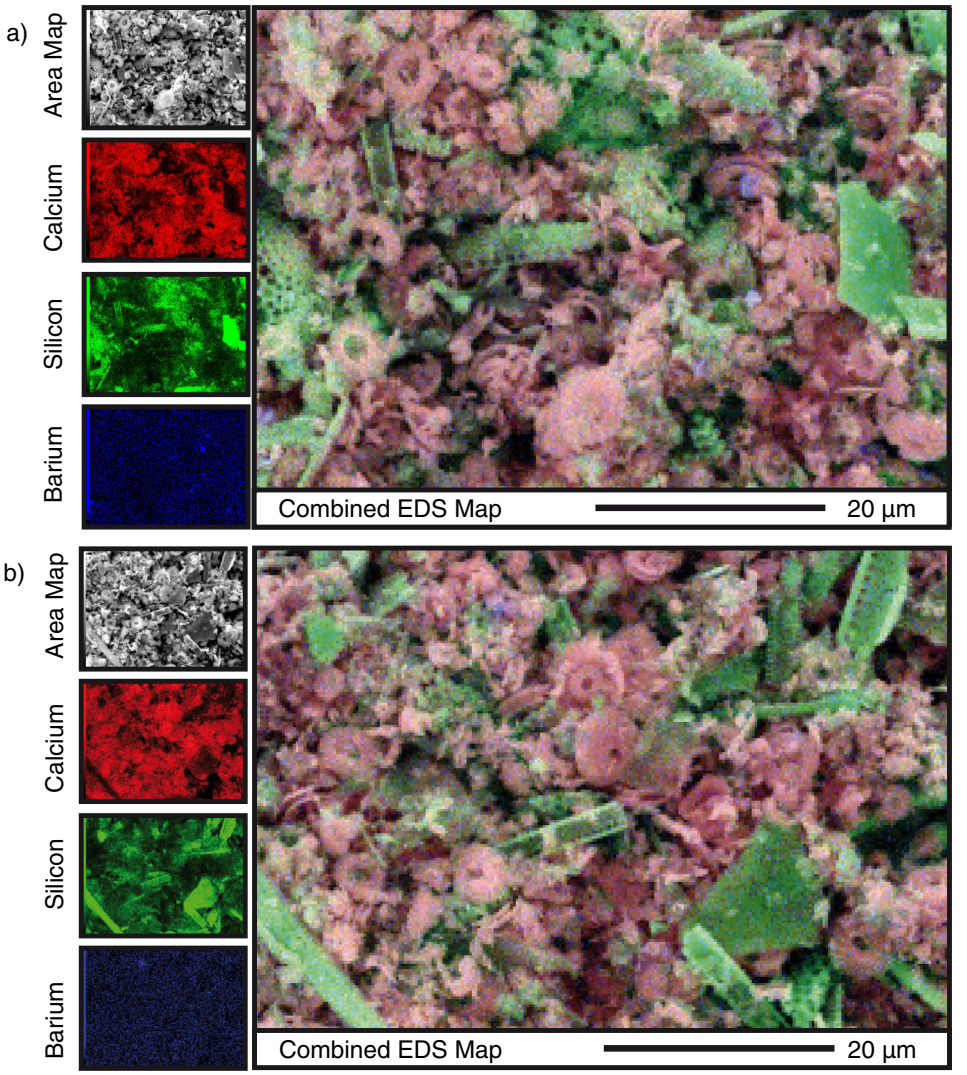



**Figure 4.** Two examples of overlays of the Ba, Ca, and Si on the SE images (sample c2, 2–5 $\mu$m fraction). These EDS maps show that the main two components are biogenic $SiO_2$ and $CaCO_3$ (O distribution not shown), (a) with marine barite present in some maps.

technique, such as the *Minoletti et al*. [2009] microfiltration technique used by *Rousselle et al*. [2013], might be more successful at isolating narrow size fractions. Ascertaining the origin of the $<2$ $\mu$m particles is not possible based on the SEM images alone, as the fragments are commonly too small to accurately determine the provenance (Figure 3). However, as the SEM images show some evidence for fragmentation of heterococcoliths (Figure 3), it is conceivable that some of the $<2$ $\mu$m particles could be fragmented holococcolith and heterococcolith, especially as holococcoliths are known to be poorly preserved in calcareous-rich sediments [*Schmidt et al*., 2006; *Bown et al*., 2008].

We expect that the isotopic ratios of samples c1 and c2 will be similar to the selected samples from *Rousselle et al*. [2013], as the coeval samples are separated by less than 4 cm ($<$2.5 kyr; supporting information Table S2). This expectation is confirmed by the close agreement between both studies for the 2–5 $\mu$m fraction $\delta^{18}O$ data, particularly for sample c1 (Figure 6a). The small offset (0.1‰) between the 2 and 5 $\mu$m $\delta^{18}O$ values of sample c2 is within error of both measurements. The offset may nonetheless reflect a small difference in depth (3–4 cm) and age (2.6–1.5 kyr) between the two studies (see supporting information Table S2), or perhaps arise from the 25% difference in coccolith amount discussed above. However, as the offset is within measurement uncertainty, we consider that the two samples are similar and can still be compared with respect to SSTs. Larger compositional differences are observed between the $\delta^{18}O$ values of the bulk

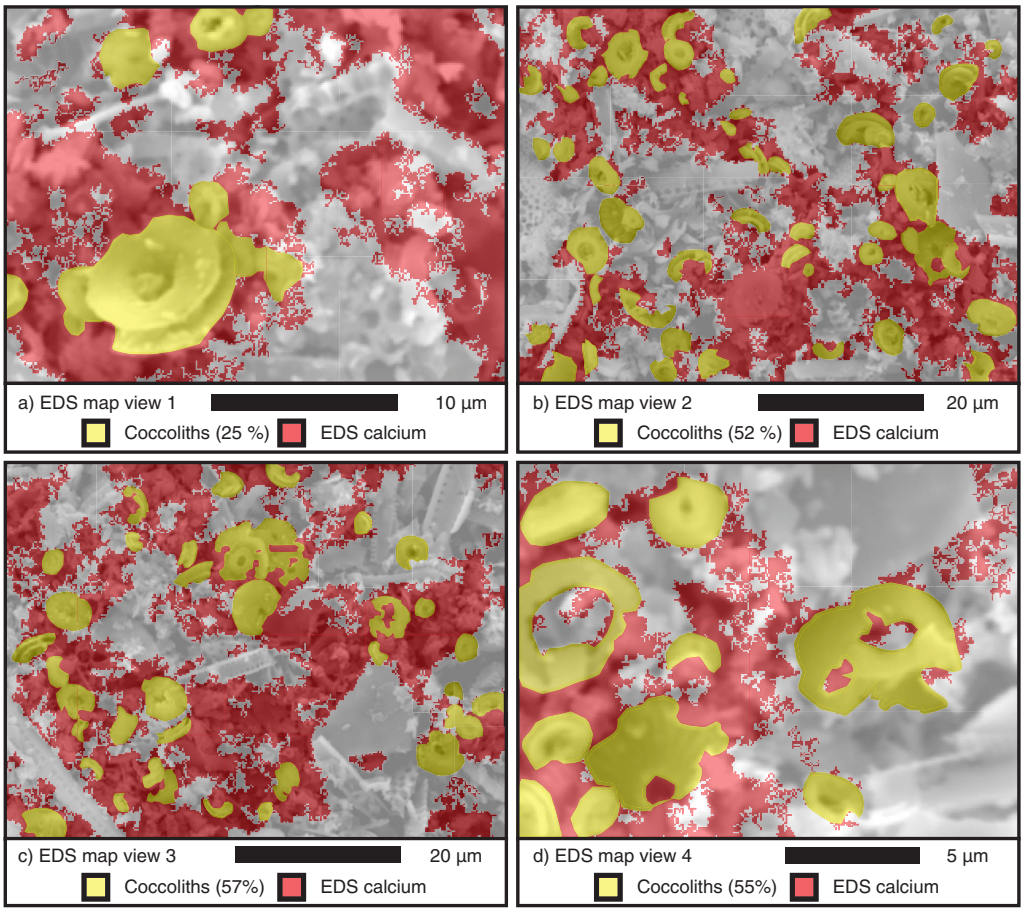



**Figure 5.** Overview of area analyses performed using the four measured EDS-SEM Ca element maps, overlaid on the original area SE-SEM images (sample c2, 2–5 $\mu$m size fraction). The red area of each map is the extent of calcium in the area. The yellow areas are the particles clearly identifiable as coccolith calcite or fragments. The EDS maps of (b and c) views 2 and 3 are presented in this study, the EDS maps of (a and d) views 1 and 4 were first presented in *Drury et al.* [2014].

[*Rousselle et al.*, 2013] and the $<$63 $\mu$m fractions (this study) of contemporaneous samples (Figures 6a and 6b), with the *Rousselle et al.* [2013] study reporting higher values (0.2–0.4‰). The higher bulk $\delta^{18}$O could reflect a greater portion of $>$63 $\mu$m benthic or thermocline planktic foraminifera in the *Rousselle et al.* [2013] samples, which precipitate at lower temperatures (higher $\delta^{18}$O), and which would, on average, give higher $\delta^{18}$O values compared to the coeval samples from this study. Published deep-sea benthic foraminiferal $\delta^{18}$O and $\delta^{13}$C values from samples c1 and c2 (c1: $\delta^{13}C = 0.18‰$, $\delta^{18}O = 3.25‰$; c1: $\delta^{13}C = -0.47‰$, $\delta^{18}O = 3.36‰$) [*Drury et al.*, 2016] are both much higher for $\delta^{18}$O and much lower for $\delta^{13}$C compared to the fine fraction data. These large differences between fine and benthic $\delta^{18}$O and $\delta^{13}$C values additionally suggest that the fine fractions predominantly represent a surface water signal.

The trends in the isotope ratios ($\delta^{18}$O, $\delta^{13}$C, and $\Delta_{47}$) as a function of size fraction can help to identify the size fraction that best represents the SST signal (Figure 6). For $\delta^{18}$O, removing benthic fragments would generate an expected trend of lower $\delta^{18}$O with smaller size fractions. However, the $\delta^{18}$O values are within error across all size fractions. Also, the average $\delta^{18}$O values are lower in samples c1 and c2, compared to the bulk $\delta^{18}$O values from *Rousselle et al.* [2013], which implies that the majority of benthic fragments were indeed removed from the $<$63 $\mu$m and smaller size fractions. For $\Delta_{47}$, removing benthic fragments would generate an expected trend of lower $\Delta_{47}$ (higher temperatures) with smaller size fractions. The visible trends in $\Delta_{47}$ are unexpected, as both samples show a slight increasing trend in $\Delta_{47}$ with decreasing size fraction. We note, however, that the sample c1 $\Delta_{47}$ measurements are mostly within error between size fractions. Interestingly, the warmer c1 $\Delta_{47}$-derived temperatures compared to that from c2 are compatible with

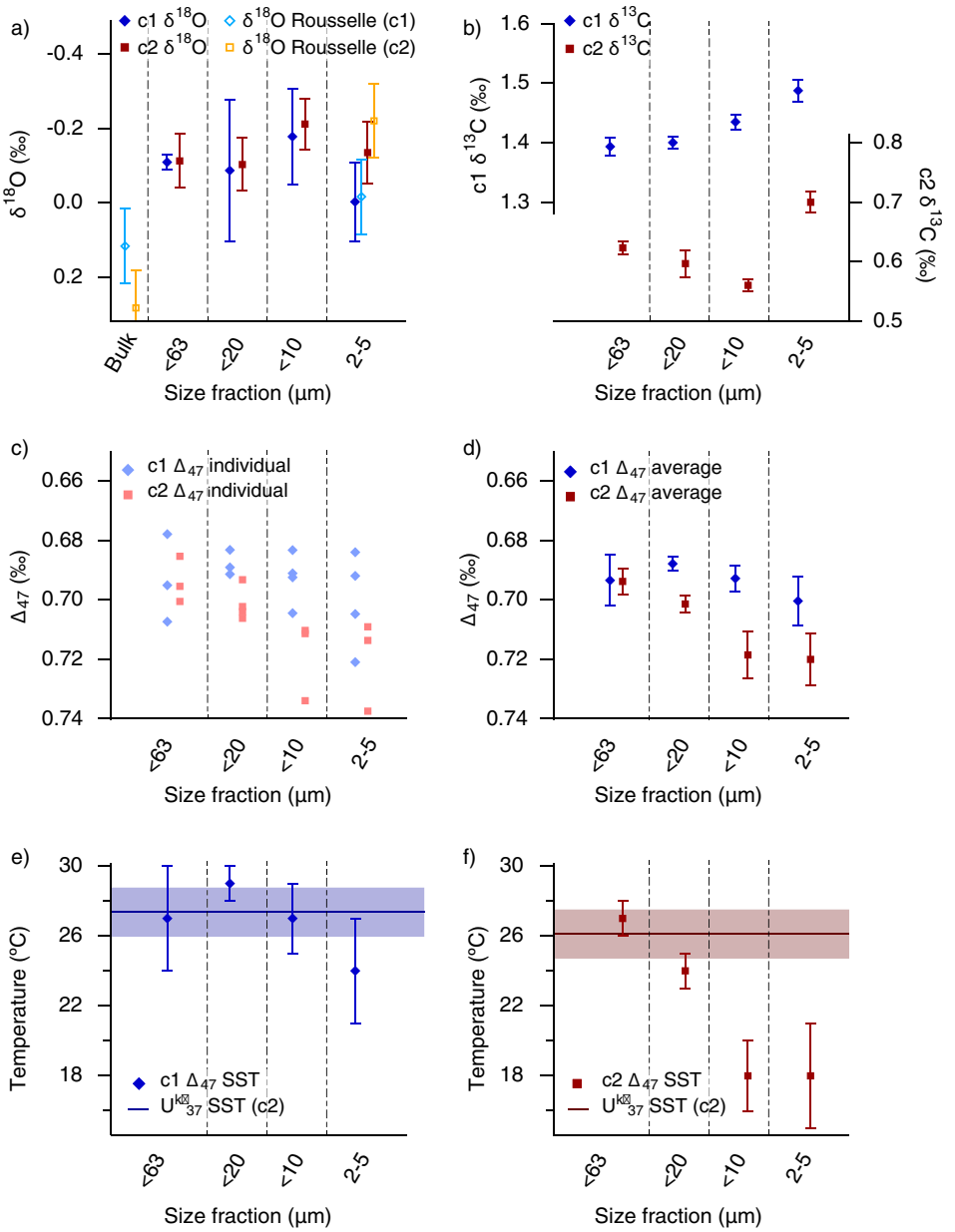



**Figure 6.** Comparison of the (a) $\delta^{18}O$ and (b) $\delta^{13}C$ results from the four size fractions from sample c1 (blue) and c2 (red) to the (a) bulk and 2–5 $\mu$m $\delta^{18}O$ from contemporaneous samples from *Rousselle et al.* [2013]. (c and d) The $\Delta_{47}$ of c1 and c2 are also shown. The comparison of the (e) c1 and (f) c2 $\Delta_{47}$-derived temperatures to $U^{k'}_{37}$ temperatures are also shown with the uncertainty marked as a broad band (derived from external precision for $U^{k'}_{37}$ temperatures reported in *Rousselle et al.* [2013]). Error bars in Figures 6a and 6b are 1 standard deviation (1 $\sigma$). Error bars for $\Delta_{47}$ in Figures 6d–6f are 1 standard error.

observations based on $U^{k'}_{37}$ [*Rousselle et al.*, 2013], which show that sample c1 was deposited at a warmer time than sample c2.

### 4.2. SST Comparisons of $\Delta_{47}$-Derived and $U^{k'}_{37}$-Derived Temperatures

The sample c1 $\Delta_{47}$-derived temperatures are within error of the concurrent $U^{k'}_{37}$ SST (~27°C) [*Rousselle et al.*, 2013] (Figure 6e). The 2–5 $\mu$m clumped temperature is slightly cooler but still within error (1.2°C for $U^{k'}_{37}$ and 3°C for $\Delta_{47}$; Figure 6e). The sample c2 $\Delta_{47}$-derived temperatures for the <63 and <20 μm fractions are also within error of the $U^{k'}_{37}$ SST (~26°C) [*Rousselle et al.*, 2013]. However, the temperatures obtained for the <10 and 2–5 $\mu$m fractions (18°C) are 8°C cooler than the $U^{k'}_{37}$ SST (Figure 6f) and unrealistically low for the surface waters of the equatorial Pacific. The 8°C offset cannot be due to the 2.42 kyr age difference between sample

c2 and the *Rousselle et al*. [2013] sample: firstly, an 8°C change is unlikely to occur so rapidly; secondly, an temporal-driven 8°C offset would affect all size fractions, whereas the $\Delta_{47}$-derived temperatures for the <63 and <20 $\mu$m fractions agree with the $U^{k'}_{37}$ SST. Several factors may affect the $\Delta_{47}$ values of the 2–5 $\mu$m calcite fraction of sample c2 and could account for the observed temperature offset: (1) coccolith vital effects; (2) coccolith preservation; and (3) the presence of abiotic/diagenetic calcite grains.

#### 4.2.1. Coccolith Vital Effects

The average $\Delta_{47}$ of the coccolith-calcite could be affected by "vital effects," which occur as coccolithophores precipitate their calcite exoskeletons and could fractionate the $\Delta_{47}$ values relative to inorganic calcite. Differences in pH between seawater and the internal vesicle where coccoliths are precipitated [*Stoll et al*., 2012] could drive $\Delta_{47}$ offsets due to vital effects. The exact pH of the vesicle is not well constrained, although research suggests that the pH can be as low as 6.4–7.2, or, in some instances, 7.6–8.3 or higher [*Anning et al*., 1996; *Stoll et al*., 2012]. A combination of vesicle pH and cell size is known to induce a "vital effect" fractionation of up to 5‰ in $\delta^{18}O$ and $\delta^{13}C$ values [*Ziveri et al*., 2003]. *Bolton and Stoll* [2013] show that there is a sudden spread in the $\delta^{18}O$ and $\delta^{13}C$ stable isotope fractionation between different size coccolith(ophores) between 7.0 and 5.0 Ma, which coincides with the interval where $\Delta_{47}$ was measured at Site U1338. The same mechanism that drives the fractionation in the conventional stable isotopes might also drive fractionation in the $\Delta_{47}$. However, most biogenic material, including coccolithophores [*Tripati et al*., 2010], indicate that vital effects do not occur in biogenic $\Delta_{47}$. In addition, research has shown that pH ranges found in the ocean (7.6–8.6 [*Stoll et al*., 2012]) is unlikely to cause additional fractionation of $\Delta_{47}$ [*Tripati et al*., 2010], although the full effects of higher or lower pH on $\Delta_{47}$ are not yet fully understood.

#### 4.2.2. Coccolith Preservation

Coccolith preservation could also affect the overall sample $\Delta_{47}$ value, as dissolution, overgrowth and recrystallization at bottom water temperatures (BWT) would reduce the contribution of surface water calcite to the overall $\Delta_{47}$. Coccospheres consist of holococcoliths and heterococcoliths [*Young et al*., 2005]. Holococcoliths consist of 0.1 $\mu$m euhedral calcite crystals and are rarely well preserved in deep-sea sediment, as the small crystal size is very susceptible to dissolution, whereas heterococcoliths consist of larger, single calcite crystals and are less susceptible to dissolution [*Schmidt et al*., 2006; *Bown et al*., 2008]. The two main concerns with coccolith calcite are dissolution (or etching) and overgrowth [*Su et al*., 2000].

SE-SEM could not determine whether any of the large or complete heterococcolith fragments had undergone recrystallization, in agreement with previous observations by *Drury et al*. [2014]. For heterococcoliths, overgrowth with secondary, diagenetic, calcite is a larger concern than recrystallization, as overgrowth is thermodynamically more favorable [*Adelseck et al*., 1973; *Hover et al*., 2001]. As shown by *Drury et al*. [2014], the coccoliths only show moderate, or poor to moderate preservation. A few heterococcoliths in samples c1 and c2 show some evidence for secondary calcite overgrowth (Figure 3); this overgrowth would increase the diagenetic $\Delta_{47}$ contribution to the total calcite $\Delta_{47}$, which could partly explain the $\Delta_{47}$ to $U^{k'}_{37}$ temperature offset. However, as suggested by *Drury et al*. [2014], some of the small crystals visible on the surface of the heterococcoliths may also be small fragments attached to the coccolith surface, so the contribution of secondary overgrowth is small. Slight etching must have occurred, as none of the heterococcoliths have preserved delicate central structures (Figure 3) [*Drury et al*., 2014], which would also decrease the proportion of surface water calcite present in the sample.

#### 4.2.3. Presence of Abiotic/Diagenetic Calcite Within the Sample

A final mechanism to explain the observed temperature offset between the $U^{k'}_{37}$ temperature and the lower $\Delta_{47}$-derived temperature from the 2–5 $\mu$m fraction of c2 is the presence of abiotic or diagenetic calcite within the sample. The EDS maps taken on the 2–5 $\mu$m fraction of sample c2 show that the small <2 $\mu$m particles are calcitic (Figures 4 and 5) and are probably particles identified as micarb by *Rousselle et al*. [2013], following the definition of *Beltran et al*. [2009]. Although some biogenic foraminiferal fragments contribute to the noncoccolith calcite (Figure 5b), most of the noncoccolith calcite consists of the unrecognizable <2 $\mu$m fragments (Figure 3). The <2 $\mu$m fragments could be disintegrated hetero- and/or holococcoliths [*Bown et al*., 2008] or abiotic/diagenetic calcite, although this cannot be confirmed without comprehensive analyses as presented in *Beltran et al*. [2009]. If these particles were formed as micritic cements from cold pore waters during early diagenesis, or disintegrated holococcoliths that underwent recrystallization during early diagenesis in bottom water temperatures, the resulting contribution of material with higher (colder) $\Delta_{47}$ to the overall sample could account for the offset between $\Delta_{47}$- and $U^{k'}_{37}$-based SSTs. If the input of cold temperature calcite (with higher $\Delta_{47}$) originates from the smallest particles in the sediment, then the presence

of $<2$ $\mu$m fragments would also explain the slight increasing $\Delta_{47}$ trend with decreasing size fraction, as removing the larger sedimentary components increases the proportion of the smaller components. Additionally, removing the 20–10 and 10–5 $\mu$m fractions also removes larger coccoliths, as these are as large as 12 $\mu$m at this time [*Bolton and Stoll*, 2013]. This could thereby further decrease the proportion of surface water coccolith calcite in the sample relative to the proportion of bottom water calcite.

Area analysis of the Ca EDS maps of the sample c2 2–5 $\mu$m fraction shows that the average proportion of coccolith calcite in the c2 sample is $\sim 47 \pm 15\%$ (Figure 5). The calcification temperature of the noncoccolith calcite ($\sim 53 \pm 15\%$) can be approximated to determine whether the mixing of the coccolith and noncoccolith calcite can account for the observed temperature offset. The 2–5 $\mu$m fraction for sample c2 calcite has a temperature of $18 \pm 3$°C (supporting information Table S2). The coccolith calcite precipitation temperature can be inferred from the contemporaneous $U^{k'}_{37}$ temperature, which is $26.1 \pm 1.1$°C (supporting information Table S2). As the ratio of noncoccolith to coccolith calcite is known for sample c2, the potential calcification temperature of the noncoccolith calcite can be obtained: the noncoccolith calcite would have had to precipitate around $\sim 6 \pm 3$°C to account for the observed discrepancy in SSTs (supporting information Table S3). The only late Miocene estimates for deep-sea temperatures in this region come from ODP Site 806 in the Western equatorial Pacific, where Mg/Ca measurements on benthic foraminifera indicate bottom water temperatures (BWT) of $5.7 \pm 1$°C [*Lear et al*., 2002, 2003] (supporting information Table S3), which is comparable to the predicted noncoccolith calcite calcification temperature. This estimation relies on a number of assumptions, both with respect to BWT at Site U1338, and importantly, about the proportion of noncoccolith calcite present in the 2–5 $\mu$m fraction of sample c2. The noncoccolith calcite contribution is estimated based on surface area alone, and therefore does not factor in differences in thickness between for instance a foraminiferal versus a heterococcolith fragment. Equally, this analysis does not account for overlap of particles. However, despite these caveats, the outcome of the approach does suggest that as a first-order approximation, the cause of the $\Delta_{47}$-$U^{k'}_{37}$-temperature offset seen in sample c2 may be due to the presence of the small $<2$ $\mu$m particles. It would be expected that the presence of the $<2$ $\mu$m particles would also affect the $\delta^{18}$O values of the 2–5 fraction of the c2 sample. This is consistent with the $\delta^{18}$O values of the 2–5 $\mu$m fraction of the c2 sample being similar, but slightly offset to higher values than the coeval sample from *Rousselle et al*. [2013], which contained on average 75% coccolith calcite, together with some micarb. Therefore, the *Rousselle et al*. [2013] $\delta^{18}$O could also have been affected by the presence of 25% particles precipitated at BWT. However, in contrast to the $\Delta_{47}$-derived temperatures, the presence of BWT particles would not have affected the $U^{k'}_{37}$-derived temperatures. Therefore, we conclude that the most likely explanation for the $\Delta_{47}$-$U^{k'}_{37}$-temperature offset is the presence of small abiotic/diagenetic calcite particles precipitated or fragmented holococcoliths recrystallized at cooler temperatures.

Of these three mechanisms, a combination of the presence of abiotic/diagenetic calcite and moderate sample preservation is the most likely explanation of the $\Delta_{47}$-$U^{k'}_{37}$-temperature offset. We also note that isolating progressively smaller size fractions could remove larger coccoliths, thereby reducing the proportion of surface water to bottom water calcite. This progressive removal of larger coccoliths with smaller size fraction could explain the observed increasing $\Delta_{47}$ trend with decreasing size fraction.

## 5. Conclusions

SEM investigations show that the technique for separating progressively smaller size fractions was successful, with the exception of the complete removal of $<2$ $\mu$m particles. The trends in $\Delta_{47}$-derived temperatures between sample c1 and c2 are consistent with sample c1 being warmer than c2. However, for both sample c1 and c2, $\Delta_{47}$-derived temperatures display a slight increasing trend with decreasing size fraction, which was unexpected, as the removal of larger size fractions should remove benthic foraminiferal fragments. The observed trend of increasing $\Delta_{47}$ with decreasing size fraction could be associated with the removal of larger coccoliths present in the 20–10 and 10–5 $\mu$m fractions. The sample c1 $\Delta_{47}$-derived temperatures are comparable to the coeval $U^{k'}_{37}$ SST ($\sim$27°C). The sample c2 $\Delta_{47}$-derived temperatures from the $<20$, $<10$, and 2–5 $\mu$m fractions are consistently cooler than the concurrent $U^{k'}_{37}$ SST ($\sim$26°C), and is too large to be attributed to a change in SST due to the small temporal offset between samples. The $\Delta_{47}$ lower temperatures are interpreted as arising from the presence of almost $\sim$53% of noncoccolith calcite in the sample c2 2–5 $\mu$m sediment fraction. If these particles reflect calcite precipitated at $\sim 6 \pm 3$°C, either as small abiotic/diagenetic

calcite particles/cements or through the recrystallization of fragmented holococcoliths, the offset between the $\Delta_{47}$- and $U^{k'}_{37}$-based SSTs can be explained.

This study has shown that coccolith-rich sediment fractions have potential as an SST proxy. We conclude that removing the >63 $\mu$m fraction will result in the removal of most nonmixed layer components, as the $\delta^{18}O$ values of the <63 $\mu$m size fraction (this study) are substantially lower than the $\delta^{18}O$ of the bulk size fraction [*Rousselle et al.*, 2013]. At the investigated site, the <63 μm size fraction are consistent between the $\Delta_{47}$ and $U^{k'}_{37}$ proxies for both samples and isolating size fractions smaller than <63 $\mu$m resulted in artificially lower SSTs for carbonate-based proxies: we thus recommend using clumped isotopes on the <63 $\mu$m fraction. The results of this study imply that $\Delta_{47}$-temperatures on coccolith-rich calcite merits further development as an SST proxy, and could be a highly valuable proxy in tropical regions where existing proxies have limitations. We caution that the size-fraction-specific composition of each location should be investigated before this method is applied, in order to select an appropriate fraction that incorporates the coccolith size range appropriate for the region and time interval.

**Acknowledgments**

This work used samples provided by the Integrated Ocean Drilling Program (IODP) and the IODP Gulf Coast Repository (GCR). The R/V JOIDES Resolution Expedition 320/321 science party members are acknowledged for their effort in collecting the material used in this study. G. Rousselle is thanked for her help in ensuring proximal samples could be chosen for comparison to their study. A. Dale, S. Davis, T. Kluge, and J. MacDonald are thanked for their help and guidance in the laboratory. T. Kluge, T. van de Flierdt, and B. Wade are thanked for providing constructive and critical feedback that helped this work. A. R. Chivas and a second anonymous reviewer are thanked for their invaluable suggestions that helped to improve this manuscript. A. J. Drury was funded by a Janet Watson studentship from Imperial College London, and the SEM work was partially facilitated by a European Consortium for Ocean Research Drilling (ECORD) research grant received by A.J. Drury in 2012. All data shown in the tables and figures are available at G$^3$ as in the supporting information, and on PANGAEA (https://doi.pangaea.de/10.1594/PANGAEA.865019), where the raw SEM export files are also provided.

## References

Adelseck, C. G., G. W. Geehan, and P. H. Roth (1973), Experimental evidence for the selective dissolution and overgrowth of calcareous nannofossils during diagenesis, *Geol. Soc. Am. Bull.*, *84*(8), 2755–2762, doi:10.1130/0016-7606(1973)84 < 2755:EEFTSD>2.0.CO;2.

Anning, T., N. Nimer, M. J. Merrett, and C. Brownlee (1996), Costs and benefits of calcification in coccolithophorids, *J. Mar. Syst.*, *9*(1-2), 45–56, doi:10.1016/0924-7963(96)00015-2.

Beltran, C., M. de Rafélis, A. Person, F. Stalport, and M. Renard (2009), Multiproxy approach for determination of nature and origin of carbonate micro-particles so-called "micarb" in pelagic sediments, *Sediment. Geol.*, *213*(1-2), 64–76, doi:10.1016/j.sedgeo.2008.11.004.

Bolton, C. T., and H. M. Stoll (2013), Late Miocene threshold response of marine algae to carbon dioxide limitation, *Nature*, *500*(7464), 558–562, doi:10.1038/nature12448.

Bown, P. R., et al. (2008), A Paleogene calcareous microfossil Konservat-Lagerstatte from the Kilwa Group of coastal Tanzania, *Geol. Soc. Am. Bull.*, *120*(1-2), 3–12, doi:10.1130/B26261.1.

Dale, A., C. M. John, P. S. Mozley, P. C. Smalley, and A. H. Muggeridge (2014), Time-capsule concretions: Unlocking burial diagenetic processes in the Mancos Shale using carbonate clumped isotopes, *Earth Planet. Sci. Lett.*, *394*, 30–37, doi:10.1016/j.epsl.2014.03.004.

Dennis, K. J., and D. P. Schrag (2010), Clumped isotope thermometry of carbonatites as an indicator of diagenetic alteration, *Geochim. Cosmochim. Acta*, *74*(14), 4110–4122, doi:10.1016/j.gca.2010.04.005.

Dennis, K. J., H. P. Affek, B. H. Passey, D. P. Schrag, and J. M. Eiler (2011), Defining an absolute reference frame for "clumped" isotope studies of $CO_2$, *Geochim. Cosmochim. Acta*, *75*(22), 7117–7131, doi:10.1016/j.gca.2011.09.025.

Drury, A. J., G. P. Lee, G. M. Pennock, and C. M. John (2014), Data report: Late Miocene to early Pliocene coccolithophore and foraminiferal preservation at Site U1338 from scanning electron microscopy, in *Proceedings of the Integrated Ocean Drilling Program*, vol. 320/321, edited by H. Pälike et al., pp. 1–14, Ocean Drill. Program, College Station, Tex.

Drury, A. J., C. M. John, and A. E. Shevenell (2016), Evaluating climatic response to external radiative forcing during the late Miocene to early Pliocene: New perspectives from eastern equatorial Pacific (IODP U1338) and North Atlantic (ODP 982) locations, *Paleoceanography*, *31*, 167–184, doi:10.1002/2015PA002881.

Duplessy, J.-C., C. Lalou, and A. C. Vinot (1970), Differential isotopic fractionation in Benthic foraminifera and paleotemperatures reassessed, *Science*, *168*(3928), 250–251.

Eiler, J. M. (2007), "Clumped-isotope" geochemistry—The study of naturally-occurring, multiply-substituted isotopologues, *Earth Planet. Sci. Lett.*, *262*(3-4), 309–327, doi:10.1016/j.epsl.2007.08.020.

Eiler, J. M., and E. Schauble (2004), $^{18}O^{13}C^{16}O$ in Earth's atmosphere, *Geochim. Cosmochim. Acta*, *68*(23), 4767–4777, doi:10.1016/j.gca.2004.05.035.

Emiliani, C. (1954), Depth habitats of some species of pelagic foraminifera as indicated by oxygen isotope ratios, *Am. J. Sci.*, *252*, 149–158.

Epstein, S., R. Buchsbaum, H. A. Lowenstam, and H. C. Urey (1953), Revised carbonate-water isotopic temperature scale, *Geol. Soc. Am. Bull.*, *64*(11), 1515–1326, doi:10.1130/0016-7606(1953)64.

Expedition 320/321 Scientists (2010), Site U1338, in *Proceedings of the Integrated Ocean Drilling Program*, vol. 320/321, edited by H. Pälike et al., pp. 1–148, Ocean Drill. Program, College Station, Tex.

Ghosh, P., J. Adkins, H. Affek, B. Balta, W. F. Guo, E. A. Schauble, D. Schrag, and J. M. Eller (2006), $^{13}C$-$^{18}O$ bonds in carbonate minerals: A new kind of paleothermometer, *Geochim. Cosmochim. Acta*, *70*(6), 1439–1456, doi:10.1016/j.gca.2005.11.014.

Grauel, A. L., T. W. Schmid, B. Hu, C. Bergami, L. Capotondi, L. P. Zhou, and S. M. Bernasconi (2013), Calibration and application of the "clumped isotope" thermometer to foraminifera for high-resolution climate reconstructions, *Geochim. Cosmochim. Acta*, *108*, 125–140, doi:10.1016/j.gca.2012.12.049.

Guo, W., J. L. Mosenfelder, W. A. Goddard, and J. M. Eiler (2009), Isotopic fractionations associated with phosphoric acid digestion of carbonate minerals: Insights from first-principles theoretical modeling and clumped isotope measurements, *Geochim. Cosmochim. Acta*, *73*(24), 7203–7225, doi:10.1016/j.gca.2009.05.071.

Herbert, T. D. (2003), Alkenone paleotemperature determinations, in *Treatise on Geochemistry*, chap. 6.15, pp. 391–432, Pergamon, Oxford.

Hover, V. C., L. M. Walter, and D. R. Peacor (2001), Early marine diagenesis of biogenic aragonite and Mg-calcite: New constraints from high-resolution STEM and AEM analyses of modern platform carbonates, *Chem. Geol.*, *175*(3-4), 221–248, doi:10.1016/s0009-2541(00)00326-0.

Huntington, K. W., et al. (2009), Methods and limitations of "clumped" $CO_2$ isotope $\Delta_{47}$ analysis by gas-source isotope ratio mass spectrometry, *J. Mass Spectrom.*, *44*(9), 1318–1329, doi:10.1002/jms.1614.

James, R. H., and W. E. N. Austin (2008), Biogeochemical controls on palaeoceanographic environmental proxies: A review, in *Biogeochemical Controls on Palaeoceanographic Environmental Proxies*, vol. 303, edited by W. E. N. Austin and R. H. James, pp. 3–32, Geol. Soc., London.

Kim, S. T., A. Mucci, and B. E. Taylor (2007), Phosphoric acid fractionation factors for calcite and aragonite between 25 and 75 degrees C: Revisited, *Chem. Geol.*, *246*(3-4), 135–146, doi:10.1016/j.chemgeo.2007.08.005.

Kluge, T., C. M. John, A.-L. Jourdan, S. Davis, and J. Crawshaw (2015), Laboratory calibration of the calcium carbonate clumped isotope thermometer in the 25–250°C temperature range, *Geochim. Cosmochim. Acta*, *157*, 213–227, doi:10.1016/j.gca.2015.02.028.

Lear, C. H., Y. Rosenthal, and N. Slowey (2002), Benthic foraminiferal Mg/Ca-paleothermometry: A revised core-top calibration, *Geochim. Cosmochim. Acta*, *66*(19), 3375–3387, doi:10.1016/s0016-7037(02)00941-9.

Lear, C. H., Y. Rosenthal, and J. D. Wright (2003), The closing of a seaway: Ocean water masses and global climate change, *Earth Planet. Sci. Lett.*, *210*(3-4), 425–436, doi:10.1016/s0012-821x(03)00164-x.

Locarnini, R. A., A. V. Mishonov, J. I. Antonov, T. P. Boyer, H. E. Garcia, O. K. Baranova, M. M. Zweng, and D. R. Johnson (2010), *World Ocean Atlas 2009*, vol. 1, *Temperature, NOAA Atlas NESDIS 68*, edited by S. Levitus, 184 pp., Government Printing Office, Washington, D. C.

Meckler, A. N., M. Ziegler, M. I. Millán, S. F. M. Breitenbach, and S. M. Bernasconi (2014), Long-term performance of the Kiel carbonate device with a new correction scheme for clumped isotope measurements, *Rapid Commun. Mass Spectrom.*, *28*(15), 1705–1715, doi:10.1002/rcm.6949.

Minoletti, F., M. Hermoso, and V. Gressier (2009), Separation of sedimentary micron-sized particles for palaeoceanography and calcareous nannoplankton biogeochemistry, *Nat. Protoc.*, *4*(1), 14–24, doi:10.1038/nprot.2008.200.

Moore, D. M., and R. C. Reynolds Jr. (1997), *X-Ray Diffraction and the Identification and Analysis of Clay Minerals*, Oxford University Press, Oxford, N. Y.

Pälike, H., M. Lyle, H. Nishi, I. Raffi, K. Gamage, A. Klaus, E. 320/321 Scientists, and Expedition 320/321 Scientists (2010), Expedition 320/321 Summary, in *Proceedings of the Integrated Ocean Drilling Program*, vol. 320, edited by H. Pälike et al., pp. 2–141, Ocean Drill. Program, College Station, Tex.

Rommerskirchen, F., T. Condon, G. Mollenhauer, L. Dupont, and E. Schefuss (2011), Miocene to Pliocene development of surface and subsurface temperatures in the Benguela Current system, *Paleoceanography*, *26*, PA3216, doi:10.1029/2010PA002074.

Rousselle, G., C. Beltran, M. A. Sicre, I. Raffi, and M. De Rafelis (2013), Changes in sea-surface conditions in the Equatorial Pacific during the middle Miocene-Pliocene as inferred from coccolith geochemistry, *Earth Planet. Sci. Lett.*, *361*, 412–421, doi:10.1016/j.epsl.2012.11.003.

Ryan, W. B. F., et al. (2009), Global multi-resolution topography synthesis, *Geochem. Geophys. Geosyst.*, *10*, Q03014, doi:10.1029/2008GC002332.

Schauble, E. A., P. Ghosh, and J. M. Eiler (2006), Preferential formation of C-13-O-18 bonds in carbonate minerals, estimated using first-principles lattice dynamics, *Geochim. Cosmochim. Acta*, *70*(10), 2510–2529, doi:10.1016/j.gca.2006.02.011.

Schmidt, D. N., D. Lazarus, J. R. Young, and M. Kucera (2006), Biogeography and evolution of body size in marine plankton, *Earth Sci. Rev.*, *78*(3-4), 239–266, doi:10.1016/j.earscirev.2006.05.004.

Spero, H. J., and D. W. Lea (1993), Intraspecific stable-isotope variability in the planktic foraminifera *Globigerinoides sacculifer*: Results from laboratory experiments, *Mar. Micropaleontol.*, *22*(3), 221–234, doi:10.1016/0377-8398(93)90045-Y.

Stoll, H., G. Langer, N. Shimizu, and K. Kanamaru (2012), B/Ca in coccoliths and relationship to calcification vesicle pH and dissolved inorganic carbon concentrations, *Geochim. Cosmochim. Acta*, *80*, 143–157, doi:10.1016/j.gca.2011.12.003.

Su, X., K.-H. Baumann, and J. Thiede (2000), Calcareous nannofossils from Leg 168: Biochronology and diagenesis, in *Proceedings of the Ocean Drilling Program, Scientific Results*, vol. 168, edited by A. Fisher, E. E. Davis, and C. Escutia, pp. 39–49, Ocean Drill. Program, College Station, Tex.

Tripati, A. K., R. A. Eagle, N. Thiagarajan, A. C. Gagnon, H. Bauch, P. R. Halloran, and J. M. Eiler (2010), C-13-O-18 isotope signatures and "clumped isotope" thermometry in foraminifera and coccoliths, *Geochim. Cosmochim. Acta*, *74*(20), 5697–5717, doi:10.1016/j.gca.2010.07.006.

Urey, H. C. (1947), The thermodynamic properties of isotopic substances, *J. Chem. Soc.*, *1947*, 562–581, doi:10.1039/jr9470000562.

Wacker, U., J. Fiebig, and B. R. Schoene (2013), Clumped isotope analysis of carbonates: comparison of two different acid digestion techniques, *Rapid Commun. Mass Spectrom.*, *27*(14), 1631–1642, doi:10.1002/rcm.6609.

Wilkens, R. H., G. R. Dickens, J. Tian, J. Backman, and E. 320/321 Scientists (2013), Data report: Revised composite depth scales for Sites U1336, U1337, and U1338, in *Proceedings of the Integrated Ocean Drilling Program, Scientific Results*, edited by H. Pälike et al., pp. 1–159, Ocean Drill. Program, College Station, Tex.

Young, J. R., M. Geisen, and I. Probert (2005), Review of selected aspects of coccolithophore biology with implications for paleobiodiversity estimation, *Micropaleontology*, *51*(4), 267–288, doi:10.2113/gsmicropal.51.4.267.

Zhang, Y. G., M. Pagani, and Z. Liu (2014), A 12-million-year temperature history of the tropical Pacific Ocean, *Science*, *344*(6179), 84–87, doi:10.1126/science.1246172.

Ziveri, P., H. Stoll, I. Probert, C. Klass, M. Geisen, G. Ganssen, and J. Young (2003), Stable isotope "vital effects" in coccolith calcite, *Earth Planet. Sci. Lett.*, *210*(1-2), 137–149, doi:10.1016/s0012-821x(03)00101-8.